ELSEVIER

Biophysical Chemistry 129 (2007) 269–278

Biophysical Chemistry

http://www.elsevier.com/locate/biophyschem

Investigation of the four cooperative unfolding units existing in the MICAL-1 CH domain

Xianju Jin, Jiahai Zhang, Haiming Dai, Hongbin Sun, Dandan Wang, Jihui Wu *, Yunyu Shi *

Hefei National Laboratory for Physical Sciences at Microscale, and School of Life Science, University of Science and Technology of China, Hefei, Anhui 230026, People's Republic of China

Received 1 March 2007; received in revised form 14 June 2007; accepted 14 June 2007
Available online 26 June 2007

Abstract

The solution structure of human MICAL-1 calpolnin homology (CH) domain is composed of six α helices and one 3_{10} helix. To study the unfolding of this domain, we carry out native-state hydrogen exchange, intrinsic fluorescence and far-UV circular dichroism experiments. The free energy of unfolding, ΔG_{H2O}, is calculated to be 7.11 ± 0.58 kcal mol^{-1} from GuHCl denaturation at pH 6.5. Four cooperative unfolding units are found using native-state hydrogen exchange experiment. Forty-seven slow-exchange residues can be studied by native-state hydrogen exchange experiments. From the concentration dependence of exchange rates, free energy of amide hydrogen with solvent, ΔG_{HX} and *m*-value (sensitivity of exposure to denaturant) are obtained, which reveal four cooperative unfolding units. The slowest exchanging protons are distributed throughout the whole hydrophobic core of the protein, which might be the folding core. These results will help us understand the structure of MICAL-1 CH domain more deeply.

Keywords: Protein folding; Native-state hydrogen exchange; Partially unfolded form; MICAL-1 CH domain

1. Introduction

Under the native conditions, many native proteins take native-like structures. In fact, some secondary structures take low free-energy native structures, while some secondary structures take relative high free-energy native-like structures. This native-state is an excited state with relatively high free energy [1,2]. The infinitesimally populated intermediates are also called partially unfolded forms (PUFs). Available results consistently indicate that protein-folding landscape is dominated by amount of metastable PUFs [3]. Traditional optical probes, circular dichroism (CD), fluorescence can not monitor these metastable PUFs. But if we use hydrogen exchange (HX) methods coupled with nuclear magnetic resonance (NMR) spectroscopy, we can detect the PUFs at atomic resolution [3,4]. Multiple PUFs have been identified by native-state HX for a number of proteins, such as cytochrome *c* [5], ribonuclease H [6], apocytochrome *b562* [7] and barnase [8].

HX results define the presence or absence of hydrogen bond of residue amides in proteins. The pattern of hydrogen bond identifies secondary structure. One can distinguish similarities and differences from the native structure under native conditions easily. In addition, native-state HX can evaluate structural stability and flexibility at an amino acid level [3]. Different secondary structures with same global unfolding free energy construct one unfolding unit. PUF is the intermediate with some units in native structure, some units in native-like structure. Investigation of unfolding unit is a way to know PUFs. In this study, we have applied native-state HX method to investigate the unfolding units of human MICAL-1 calponin homology (CH) domain.

MICAL is a family of proteins conserved in organisms ranging from flies to mammals. MICAL is first identified as CasL interacting protein. Human MICAL-1 contains an N-terminal flavoprotein monoxygenase domain, a CH domain, a LIM

Abbreviations: HX, hydrogen exchange; PUF, partially unfolded form; PF, protection factor; CH domain, calponin homology domain; CD, circular dichroism; RSA, residue solvent accessibility.

* Corresponding authors. Tel.: +86 551 3607464; fax: +86 551 3601443.
E-mail addresses: wujihui@ustc.edu.cn (J. Wu), yyshi@ustc.edu.cn (Y. Shi).

0301-4622/$ - see front matter © 2007 Elsevier B.V. All rights reserved.
doi:10.1016/j.bpc.2007.06.008

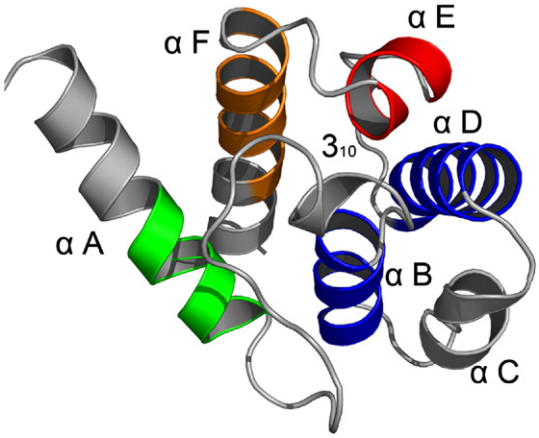

Fig. 1. Structure of human MICAL-1 CH domain. (A) Colored cartoon representation of the MICAL-1 CH domain energy-minimized average structure [11]. NMR structure of human MICAL-1 CH domain is characterized by six α helices and a 3_{10} helix. This figure was produced with PyMol from the protein NMR structure 2DK9 in the PDB.

domain, a proline-rich domain, and a coiled-coil motif. The CH domain is a potential protein–protein interaction module and may play a role in recruiting downstream effectors [9,10]. NMR study has shown that the structure of human MICAL-1 CH domain is composed of six α helices and one 3_{10} helix (Fig. 1), very similar to other CH domains (e.g. human MICAL-3 CH domain, PDB code: 2D88) [11]. The fold is dominated by four long α helices, in which three α helices, αB (residues 36–45), αD (residues 60–74) and αF (residues 91–108), are assembled into a parallel bundle and the N-terminal helix αA (residues 2–16) is packed perpendicularly. The four α helices are connected by two small α helices, αC (residues 52–58) and αE (residues 83–88), one 3_{10} helix (residues 30–32).

In our previous work, we have solved the solution structure of human MICAL-1 CH domain [11]. To understand the structural basis for the initiation of folding and to find the PUFs of the MICAL-1 CH domain, native-state HX experiments have been done in addition to intrinsic tryptophan fluorescence and far-UV CD spectroscopy. This paper is the first report on the residue-specific information of MICAL-1 CH domain stability. The hydrogen exchange free energy (ΔG_{HX}) of CH domain is investigated as a function of deuterated GuHCl (GuDCl) concentration at pD 6.6 (pD=pH+0.4). Our results clearly show that the CH domain is composed of four cooperative unfolding units. The results also indicate that hydrophobic core is the slow-exchange core, and hydrophobic interactions may be the main force to maintain the three-dimensional structure.

2. Materials and methods

2.1. Chemicals

Ultra pure GuHCl was purchased from Calbiochem. GuHCl was deuterated by dissolving in D_2O and lyophilized. This was repeated three times. GuDCl was stored in a desiccator prior to dissolution [12]. All other reagents were of analytical grade. All solutions were prepared with redistilled water and filtrated through a 0.22 μm filter membrane.

2.2. Protein expression and purification

The human MICAL-1 CH domain gene was cloned in plasmid p28 (Novagen) and expressed in BL21 (DE3) strain of *Escherichia coli.*. Recombinant MICAL-1 CH domain contained an N-terminal His tag (MGHHHHHHM) and was purified using Ni-chelating column (Qiagen). The purity of recombinant MICAL-1 CH was confirmed by Tricine-SDS-PAGE (15%, w/v) and the concentration was measured with a bicinchoninic acid (BCA) protein assay kit (Pierce), as described previously [11].

Uniformly ^{15}N-labeled MICAL-1 CH for NMR spectroscopy was grown in SV40 medium with ^{15}N-labled NH_4Cl as the only nitrogen source. Purification was carried out as described above for the unlabeled protein.

2.3. Equilibrium unfolding experiments by fluorescence and far-UV CD spectroscopy

Intrinsic fluorescence emission spectra were studied by a thermo spectronic Aminco-Bowman series2 luminescence spectrometer. The fluorescence spectra were measured at a protein concentration of 0.02 mg/ml with a 1 cm path-length cell. The emission spectra were recorded in range of 310–370 nm with the excitation wavelength at 285 nm. Each spectrum was the average of three scans. Before measurements, the protein samples were incubated at 20 °C for 2 h. Measurements were taken at 20 °C.

When the concentration of GuHCl increased, λ_{max} was red-shifted, while the fluorescence intensity only changed a little (see Results). The fraction of the unfolded protein, F_U, was calculated using the equation,

$$F_U = (f_N - f)/(f_N - f_U) \quad (1)$$

where f is the observed λ_{max} at a given GuHCl concentration, f_U is λ_{max} of the completely unfolded protein and f_N is the λ_{max} of the native protein [13]. The fluorescence spectra were corrected for the background fluorescence of the buffer.

CD measurements were carried out with a Jasco Model J-810 spectropolarimeter. Far-UV CD spectra were measured in the range 190–250 nm at a protein concentration of 0.1 mg/ml with a 0.1 cm path-length cell. Prior to measurements, the protein solutions were incubated at 20 °C for 2 h. The spectra were measured three times, averaged and corrected by subtraction of the solvent spectrum obtained under identical conditions. Results are expressed in terms of molar ellipticity (θ). The fraction of unfolded protein F_U at various GuHCl concentrations was calculated using the following equation:

$$F_U = (\theta_N - \theta)/(\theta_N - \theta_U) \quad (2)$$

where θ is the observed molar ellipticity at a given GuHCl concentration, θ_U is the molar ellipticity of the completely unfolded state, and θ_N is the molar ellipticity of the native protein. The free energy of the protein unfolding, ΔG_U, can be calculated by $\Delta G_U = -RT \ln F_U$. This ΔG_U is linearly related to the concentration of denaturant, GuHCl, as

$$\Delta G_U = \Delta G_{H_2O} - m[G_U HCl] \quad (3)$$

where ΔG_{H2O} is the apparent free energy of unfolding in the absence of denaturant and m depends on the denaturant binding surface newly exposed in the unfolding reaction [13,14].

These fluorescence and CD spectra measurements were taken in 50 mM NaCl, 50 mM PBS pH 6.5 buffer.

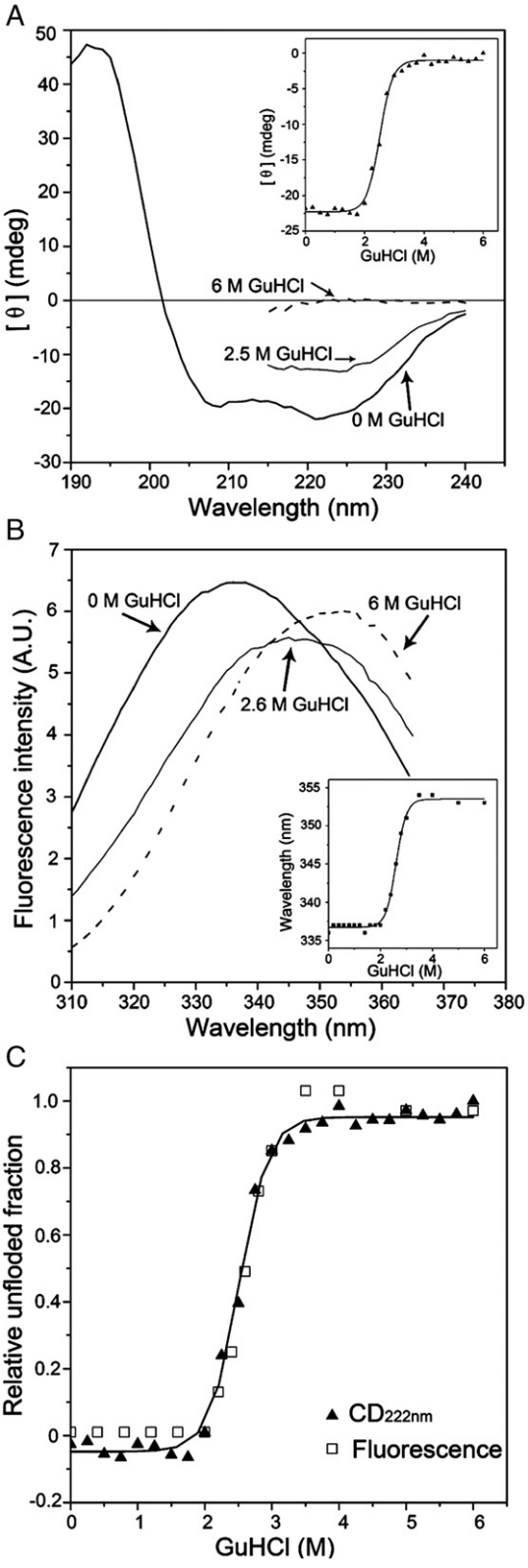

Fig. 2. The optical probes of MICAL-1 CH domain unfolding process. (A) Far-UV CD spectra of CH under native, transitional and unfolded conditions (0 M, 2.5 M and 6 M). The inset shows the GuHCl-induced unfolding transition by following the ellipticity at 222 nm. (B) Fluorescence emission spectra of CH under native, transitional and unfolded conditions (0 M, 2.6 M and 6 M). The inset shows the GuHCl-induced unfolding transition by following the maximum emission wavelength. (C) The unfolding transition curve obtained by monitoring changes of the secondary structure by following far-UV CD at 222 nm (▲). Change of the tertiary structure by following λ_{max} (□) was consistent with transition curve. The relative unfolded fraction was calculated by setting the native state value as 0 and the totally unfolded value as 1.

2.4. Native-state HX experiments

Equilibrium native-state HX experiments were carried out at various GuDCl concentrations (0–1.4 M). The final protein concentration used for NMR was typically 0.5–1 mM. Freeze-dried ^{15}N-labeled MICAL-1 CH domain was dissolved into an EX2 limit condition [15], containing 50 mM PBS (pD=6.6), 50 mM NaCl and various GuDCl concentration in D_2O solution. For each GuDCl concentration, a series of ^{1}H–^{15}N hetero-nuclear single quantum coherence (HSQC) spectra were acquired at appropriate time intervals in a Bruker 600 MHz spectrometer at 20 °C. Spectra were processed using NMRPipe and NMRDraw software [16], and the data were analyzed with SPARKY. The peak intensities in the HSQC spectra were normalized by comparing intensities of resonance in the aliphatic region of high-resolution ^{1}H–NMR spectra.

2.5. Treatment of native-state HX data

The normalized peak intensities of each amide proton, $I(t)$, was measured by heights of cross-peaks in the HSQC spectra. It obeys a single-exponential decay. The amide hydrogen-dueterium exchange rate, k_{ex}, can be then obtained by the equation

$$I(t) = I_\infty + A\exp(-k_{ex}t) \tag{4}$$

where I_∞ is the intensity at the infinite time, and A is the total change in intensity.

The values for k_{ex} are used for calculating the exchange free energy (ΔG_{HX}) with the equation,

$$\Delta G_{HX} = -RT\ \ln\ (k_{ex}/k_{int}) \tag{5}$$

where k_{int} is the intrinsic chemical exchange rate estimated for amide protons in unstructured peptides [17]. Protection factor, PF, is defined as PF=k_{int}/k_{ex} for each amide proton. ΔG_{HX} versus a profiles are commendably fitted by the following analytical expression,

$$\Delta G_{HX} = -RT\ \ln\ \{\exp((-\Delta G_{lf} + m_{lf}[GuDCl])/RT) + \exp\big(\big(-\Delta G_g + m_g[GuDCl]\big)/RT\big)\} \tag{6}$$

where ΔG_{lf} and m_{lf} are determined from the phase in low GuDCl concentration, ΔG_g and m_g are determined from the phase at relatively high GuDCl concentration. ΔG_{lf} and m_{lf} are

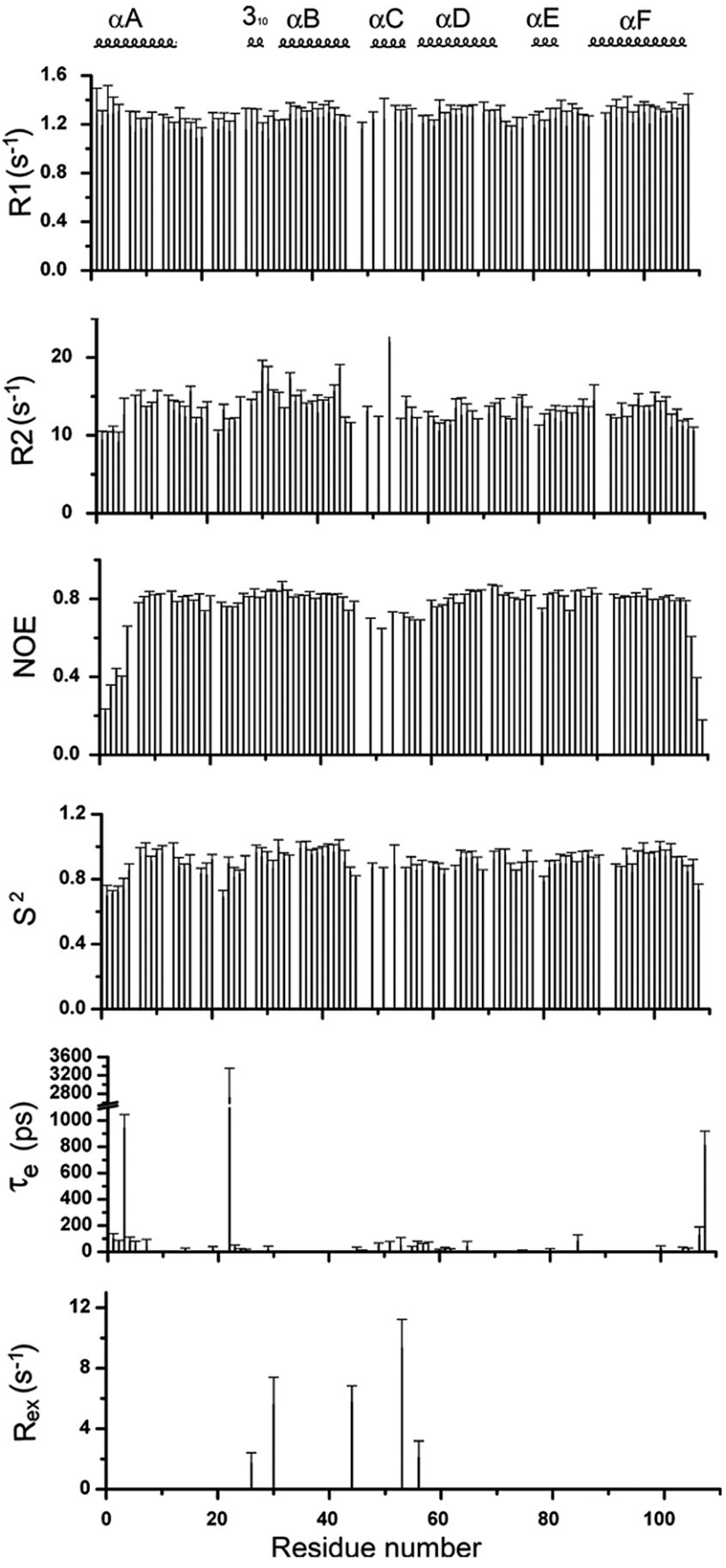

Fig. 3. Backbone dynamics of MICAL-1 CH domain. ^{15}N relaxation data of R_1, R_2 and ^1H–^{15}N NOE and S^2, τ_e and R_{ex} results of Lipari–Szabo analysis by FAST-ModelFree for MICAL-1 CH domain at 600 MHz are plotted *vs.* residue number. The secondary structure of MICAL-1 CH is indicated at the top.

the free energy and m-value of the local fluctuation, respectively. ΔG_g and m_g are the free energy and m-value of global unfolding, respectively. In practice, ΔG_g was obtained from the extrapolation of ΔG_{HX} to 0 M GuDCl from the phase at relatively high GuDCl concentration [15].

During the global unfolding, the dependence of unfolding free energy ΔG_{HX} on GuDCl concentration is often assumed to be linear,

$$\Delta G_{HX} = \Delta G_g - m[G_U DCl] \quad (7)$$

where the slope m represents the additional denaturant sensitive surface exposed in the unfolding reaction [18].

2.6. Backbone dynamic study

The $^{15}N–T_1$, $^{15}N–T_2$ and $^{1}H–^{15}N$ NOE were measured using ^{15}N-labeled MICAL-1 CH domain in H_2O buffer (10% D_2O) at 293 K with a Bruker 600 MHz spectrometer. SPARKY was used for the analysis of the relaxation data. R_1 and R_2 values were determined from the fitting of the relation of peak intensities *vs.* variable delays to a single-exponential. $^{1}H–^{15}N$ NOE values were reported as peak intensity ratios obtained with and without ^{1}H saturation. The squared order parameter (S^2), the effective correlation time for the fast internal motions (τ_e) and ^{15}N exchange broadening contributions value (R_{ex}) were obtained by fitting R_1, R_2, and NOE values in the framework of the Lipari-Szabo formalism using the FAST-Modelfree software (v1.1).

2.7. Residue solvent accessibility (RSA)

RSA was calculated using the NACESS program [19], with the PDB coordinates 2DK9.

3. Results

3.1. Unfolding process detected by far-UV CD and fluorescence spectroscopy

Equilibrium denaturation by GuHCl was monitored using far-UV CD and intrinsic fluorescence spectroscopy.

Unfolding of MICAL-1 CH domain was accompanied by large changes in far-UV CD spectra (Fig. 2A). The θ value at 222 nm was chosen as the probe of secondary structure (Fig. 2A inset). The titration could be analyzed with two states model.

Another probe, intrinsic fluorescence was also used to monitor the unfolding. The intrinsic fluorescence emission spectra of native, partially unfolded and unfolded of MICAL-1 CH proteins are shown in Fig. 2B. The fluorescence emission was red-shifted from 338 nm in the native state to 350 nm in the unfolded state. In Fig. 2B inset, we plotted λ_{max} against GuHCl concentration and analyzed the plot by two states. To compare the two titrations more directly, we normalized $\theta_{222\ nm}$ and λ_{max} as shown in Fig. 2C. As seen in the figure, the two titration curves overlapped well, and the mid-points obtained by $CD_{222\ nm}$ and λ_{max} were nearly the same, suggesting that disruption of the secondary and the tertiary structure occurred concurrently. Equilibrium unfolding of MICAL-1 CH appears to be the single transition with two well-separated states.

These experiments were repeated several times. They were in good agreement irrespective of the measurement time. Its unfolding could be treated as reversible system. Taking the slopes of the folded and unfolded baselines into account, the denaturation curves were fitted using the linear extrapolation model in order to estimate ΔG_{H2O} (the free energy of unfolding in the absence of GuHCl, see Materials and Methods) [20]. The obtained ΔG_{H2O} was 7.11±0.58 kcal mol^{-1}. The GuHCl concentration of the unfolding transition midpoint was 2.5± 0.02 M, and the m-value of Eq. (3) was 2.82±0.23 kcal $mol^{-1}M^{-1}$.

3.2. Backbone dynamic properties and solvent accessibility

MICAL-1 CH domain contains six α helices and one 3_{10} helix. Here only five α helices could be observed by the native-state HX experiment (see the native-state HX results). Residues in the N-terminal, C-terminal, 3_{10} helix and αC could not be observed. In order to solve this problem, we performed ^{15}N relaxation experiments on backbone dynamics. ^{15}N relaxation data reflects dynamic properties of the protein even though there is no direct correlation between ^{15}N relaxation data and HX data, because residues in flexible regions exchange more readily with solvent deuterium in the native-state HX experiment as solvent access to flexible regions more easily. Thus ^{15}N relaxation data can help us understand HX behaviors of some special residues.

To explore the backbone dynamics of MICAL-1 CH domain, $^{15}N–T_1$, $^{15}N–T_2$ and $^{1}H–^{15}N$ NOE experiments were performed using ^{15}N-labeled protein. Squared order parameter (S^2), the effective correlation time for fast internal motions (τ_e) and ^{15}N exchange broadening contribution (R_{ex}) values were obtained using the Lipari–Szabo model and analyzed by FAST-Modelfree program. The averaged value of NH S^2, an index of backbone motions, was obtained as 0.9 in the secondary structural region. Most residues were rigid, while some were relatively flexible. The first five residues of the N-terminal, the last three residues of the C-terminal, and the residues from αC and 3_{10} had smaller S^2 values than the average order parameter in helices (Fig. 3), indicating that these regions are relatively more flexible than the other regions.

RSA is another index for residue flexibility. Residues in the flexible region are easily accessed by solvent and exchange readily with solvent deuterium, hence have relatively high RSA (Fig. 4). So residues in the flexible region have the relatively high RSA value. The high RSA values in N-terminal, C-terminal, 3_{10} helix and αC regions indicate their relatively high flexibility attributes.

3.3. Global, sub-global, and local-fluctuation types of native-state HX

The backbone amide proton peaks in the finger-print region of 2D HSQC spectra of MICAL-1 CH were easily assigned

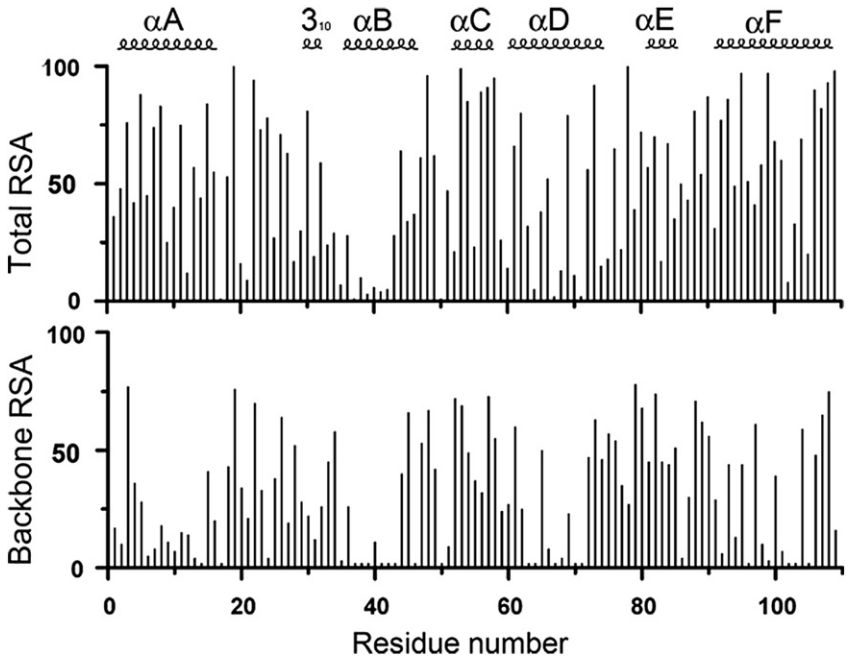

Fig. 4. Backbone RSA and total atom RSA. The residue solvent accessibilities are calculated by using the program NACCESS [19].

according to our previous work [11]. Only 47 slowe exchange backbone amide protons could be observed in this experiment (Table 1). These observed residues exhibited different hydrogen exchange behaviors. Other residues easily exchanged with deuterium and hence could not be observed in the experiment dead time. Based on the different profiles of hydrogen exchange energy ΔG_{HX} *vs.* GuDCl concentration, observed residues could be divided into three types [18]:

(1) Little dependence on GuDCl concentration. Most of these residues were in loop or helix terminal regions. HX-responsible opening reactions of these residues occurred through local fluctuation.
(2) Biphasic with near-zero *m*-values at low GuDCl concentrations and large *m*-values at higher GuDCl concentrations. The HX-responsible opening reaction changed from local fluctuation to cooperative global unfolding.
(3) Biphasic with small *m*-values at low GuDCl concentrations and large *m*-values at higher GuDCl concentration. The HX-responsible opening reaction changed from the smaller-scale unfolding event to the larger-scale one. Their HX-responsible opening reaction changed from sub-global to global unfolding.

The HX profile of each residue was assigned to one of these three types based on *m*-value and ΔG_{HX}, which could be easily obtained by Eqs. (5), (6)and (7). The HX profiles were simulated by Eq. (6)(see Materials and methods).

Table 1
Location of the seven helices, loops and turns in 3D structure of MICAL-1 CH domain

Structure	Amino-acid residues	Amino-acid residue probes
αA	2–16	R11, W12, C13, Q14, E15, Q16
3_{10} helix	30–32	W32
αB	36–45	L36, Q37, L38, C39, L41, V42, Y43, L45
αC	52–58	–
αD	60–74	A60, E62, A63, T64, A65, W66, A67, L68, K69, A71, E72, N73
αE	83–88	V86, V87, A88, G89
αF	92–108	L95, I96, A97, Y98, L99, S100, H101
Loops or turns		T17, A18, A33, G35, E74, L75, I77, V81, A85

The residues observed in native-state HX experiment and their locations are shown.

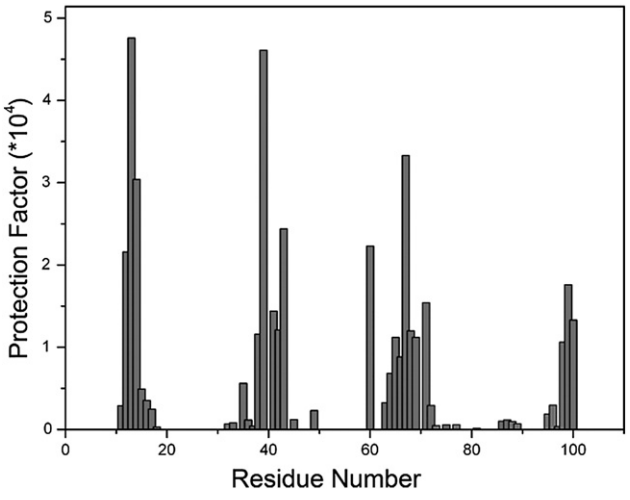

Fig. 5. The protection factors (PFs) estimated for all the observed amide protons in MICAL-1 CH domain at 0 M GuDCl.

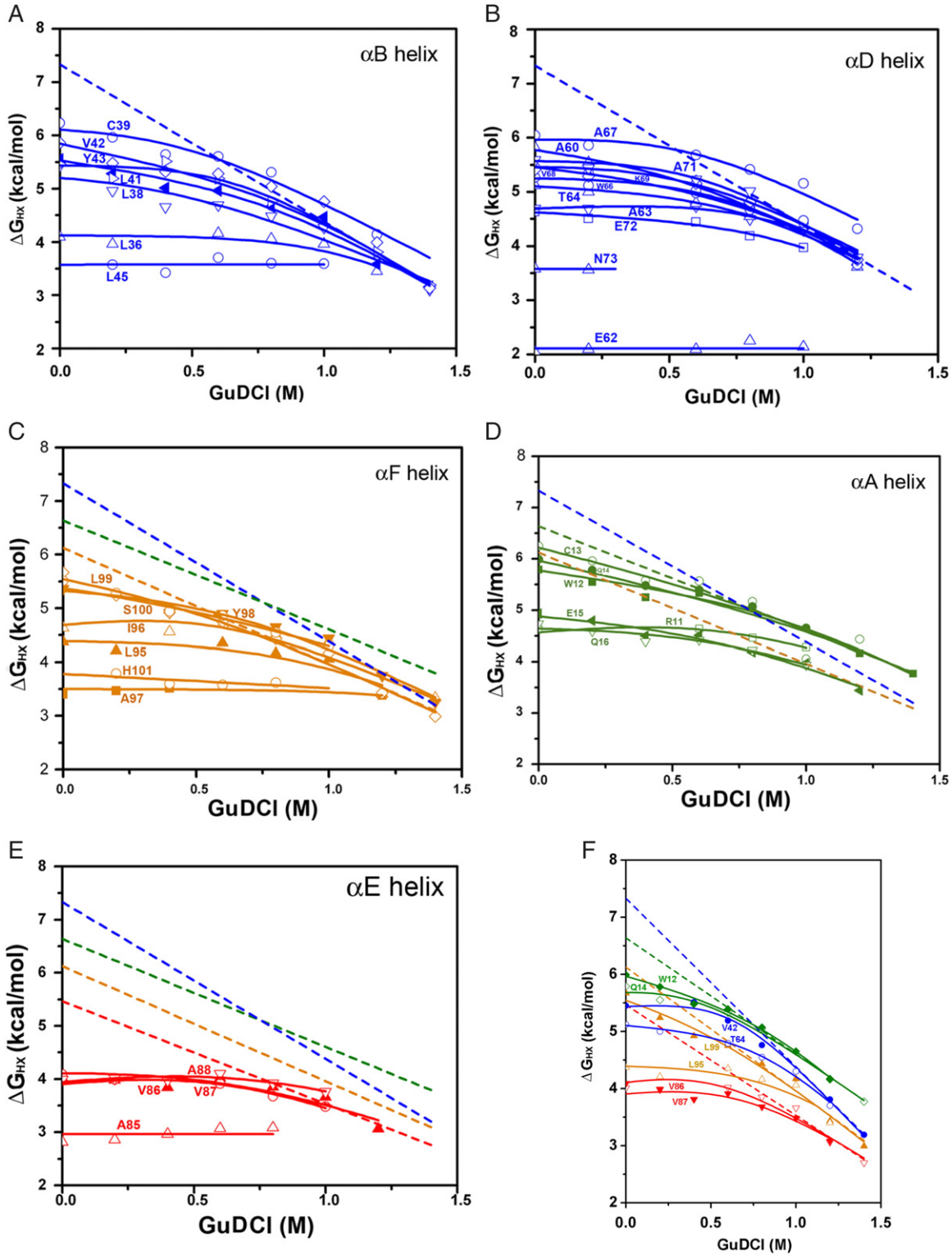

Fig. 6. HX profiles of each secondary structure. Dash line is the extrapolation line of converged profiles at higher GuDCl concentration. (A) HX profiles of αB; (B) HX profiles of αD; (C) HX profiles of αF; (D) HX profiles of αA; (E) HX profiles of αE; (F) HX profiles of typical residues of each unfolding group. (For interpretation of the references to colour in this figure legend, the reader is referred to the web version of this article.)

We found 16 residues took near-zero *m*-values in our HX data (residues T17, A18, W32, L36, L45, E62, N73, E74, L75, I77, V81, A85, A88, G89, S100 and H101), most of which were located either in a loop, or at the end of helices. They had relatively high RSA (Fig. 4), and therefore easily exposed to the solvent. They exchanged through local fluctuation without exposing significant new surface area with the increase of GuDCl concentration.

Residues in one secondary structure exhibited more than one type of HX profiles. HX profiles of the residues in the middle helix region always took sub-global to global unfolding type, and HX profiles of the residues at the terminal region of helices took local fluctuation.

3.4. HX profiles of each secondary structure

HX profiles of one secondary structure often converge to one line at relatively high concentration of GuDCl. Two different secondary structures may have the same or similar HX profiles, or significantly different HX profiles, depending mainly on their locations in the whole structure. Here we show the HX profiles of each secondary structure.

3.4.1. αB helix

Fig. 6A portrays HX of residues in αB helix. HX profiles of residues L38, C39, L41, V42 and Y43 in αB helix exhibits sub-global to global unfolding type with small *m*-values at low GuDCl concentrations and larger *m*-values at higher GuDCl concentrations [18]. Except for C39, their HX profiles converge to a line (blue dash line (Fig. 6A)) with a higher *m*-value (2.8± 0.3 kcal mol^{-1} M^{-1}) at higher GuDCl concentration. By extrapolating the converged slope at higher GuDCl concentration to zero, we obtain a ΔG_g of 7.0±0.5 kcal mol^{-1} at 0 M GuDCl. The amide proton of C39 is blocked by the side chain isobutyl of the neighboring residue L38. It is highly protected than other residues. The PF value of C39 is higher than its neighbor residues in αB helix (Fig. 5). L36 and L45 show type 1 HX behavior, while other residues (L38, C39, L41, V42, and Y43) show type 3. L36 and L45 have extremely small PFs (Fig. 5), about 40 times smaller than that of C39. Residues located at the middle part of the helix are more protected than the residues located at the end of the helix.

3.4.2. αD helix

Fig. 6B portrays HX profiles of residues in αD helix. The blue dash line in Fig. 6B is the extrapolation line of converged line at higher GuDCl concentration, almost the same as that of αB helix. HX profiles of residues A60, V62, A63, T64, W66, V68, and K69 in αD helix are the same as that of the residues in αB helix. A67 shows much more protection just as C39 does. Residues E62 and N73 exhibit the local fluctuation HX because of their end location.

3.4.3. αF helix

Fig. 6C portrays the HX profiles of residues in αF helix. Residues L95, I96, A97, Y98, L99, S100, and H101 converge to a line (orange dash line in Fig. 6C) with a *m*-value of 2.0± 0.1 kcal mol^{-1} M^{-1} at higher GuDCl concentration, and a ΔG_g of 6.2±0.2 kcal mol^{-1} at 0 M GuDCl. HX profiles of Y98, L99, and S100 can be assigned as type 3. HX profiles of I96 and L95 can be assigned as type 2. HX profiles of A97 and H101 can be assigned as type 1. Residues in the middle part of the helix and near the hydrophobic core residues (I96, L99) are more stable, while residues in the terminal part of helix are much less protected.

3.4.4. αA helix

Fig. 6D portrays the HX profiles of residues in αA helix. αA helix is the N-terminal helix of MICAL-1 CH domain. The N-terminal residues G1-L10 in αA helix are not observed by native-state HX experiment. Residues R11, W12, C13 and Q14 converge to a line (green dash line in Fig. 6D) with a *m*-value of 2.0±0.1 kcal $mol^{-1}M^{-1}$ at higher GuDCl concentration, and a ΔG_g of 6.6±0.1 kcal mol^{-1} at 0 M GuDCl. Residues E15 and Q16 are located at the end of αA helix. They have small PFs (Fig. 5), low HX energy, and are less stable than the central residues of the helix. At relatively high concentration of GuDCl, residues E15 and Q16 have not evened out for other residues of the same helix αA. It might be that the helix at E15 and Q16 region is less compact than other regions of same helix.

3.4.5. αE helix

Fig. 6E portrays HX profiles of residues in αE helix. HX profiles of residues A85, V86, V87, and A88 converge to a line (red dash line (Fig. 6)) with a *m*-value of 1.8±0.1 kcal mol^{-1} M^{-1} at higher GuDCl concentration, and a ΔG_g of 5.2±0.2 kcal mol^{-1} at 0 M GuDCl. Amide protons of A85 and A88 exchange through local fluctuation. PFs and HX free energy of αE residues exhibit much lower than other helices.

3.4.6. αC helix

Residues of αC helix (P52–L58) are not observed in native-state HX experiment. This small helix is located far away from the hydrophobic core. These residues have high RSA values (Fig. 4), and hence cannot protect their amide protons from solvent deuterium accessing.

3.4.7. 3_{10} helix

Only one residue, W32, of 3_{10} helix (S30-W32) is observed in native-state HX experiment. Its amide proton exchanges through type 1 local fluctuation (data not shown). Residue W32 is located in the small 3_{10} helix, its side chain took part in the first hydrophobic core formation.

3.4.8. Loops

Residues T17, A18, A33, G35, L75, and V81 in loop regions are observed. These residues exchange through type 1 local fluctuation (data not shown). All of them are located adjacent to helices and have weak interactions with helices residues. Therefore they can be observed while other loop residues cannot.

4. Disscussion

4.1. Residues in one secondary structure with different local stability

Exchange rates of 47 out of 109 amide protons in total can be measured at pD 6.6 at 293 K (Table 1). Sixty-two main-chain amide protons are exchanged to deuterium within the dead time of the measurement (30 min), most of which correspond to residues located in regions of flexible structure, either in the N- or C-termini, or in the loop regions.

Among the observed 47 slow exchange residues, 17 backbone amide protons are highly protected against H-D exchange (PF larger than 10^4), 12 are less protected (PF smaller than 10^3) (Fig. 5). Most of the seventeen highly protected residues, W12, C13, Q14, L38, C39, L41, V42, Y43, A60, A65, A67, L68, K69, A71, Y98, L99 and S100, are located in the middle part of helix and participated in the hydrophobic core formation [11]. Among the 12 less protected residues, A18, A33, L75, I77 and V81 are located in loop regions, Q37, E62, N73, A88, G89 and A97 in terminal regions of helices, and W32 in the 3_{10} helix.

The hydrophobic core residues are much more protected than other residues. Their hydrogen exchange rates are very slow. Woodward and co-workers have proposed that slow exchange core is the folding core, based on the studies of BPT1 [1]. In our case, the slow exchange core is also the hydrophobic core. Our finding is in agreement with Woodward's observation. The hydrophobic core residues have relatively higher HX free energy than other residues, which also indicate that they are more stable than other residues. We may say that the hydrophobic interaction is the main force to stabilize the three-dimensional structure of MICAL-1 CH domain.

4.2. Four cooperative unfolding units

The exchange rate observed of each amide proton provides an estimation of the free energy of the opening event that leads to the exchange. Hence, information about the stability units of a protein can be obtained. Our HX data segregate into distinct units (Fig. 6F). The GuDCl concentration dependent ΔG_{HX} in the observed secondary structures converge into four groups at relatively high GuDCl concentration (Fig. 6A–E). Fig. 6F shows the four representative pairs of amide protons in each group. The four groups in the figure are assigned to four different types defined above, and referred to as four units hereafter. Each unit is colored and presented in the three-dimensional structure (Fig. 1).

Residues belong to the highest energy unit portray the global unfolding equilibrium, and residues in the lower lying unit reflect partially unfolded forms [21]. At low GuDCl concentration, the exchange of most amide protons is dominated by local structural fluctuations. With the increasing of GuDCl concentration, the global unfolded state is selectively promoted. Eventually, the exchange curves merge to define a HX type that reveals the global unfolding reaction. The dash lines are the extrapolation of global unfolding merge lines, and can help us to distinguish each cooperative unfolding unit easily. For each residue, the ΔG_{HX} shows a linear dependence on GuDCl concentration. The ΔG_{HX} value at 0.0 M GuDCl represents the global unfolding free energy.

Helices αB and αD compose a cooperative unfolding unit. They converged at high GuDCl concentration (blue), with ΔG_g of 7.0±0.5 kcal mol^{-1},and *m*-value of 2.8±0.3 kcal mol^{-1} M^{-1}, which are same as the protein global unfolding free energy ΔG_{H2O} (7.11±0.58 kcal mol^{-1}) and the global unfolding *m*-value (2.82±0.23 kcal mol^{-1} M^{-1}), as detected by equilibrium unfolding probes CD and intrinsic fluorescence. Residues of αA compose an unfolding unit. The αA helix residues converge to a green blue dash line with a ΔG_g of 6.6±0.1 kcal mol^{-1} and a *m*-value of 2.0±0.1 kcal mol^{-1} M^{-1}. All the amide protons in the peptide group of αF can exchange through local fluctuation and sub-global unfolding at low GuDCl concentration, these residues compose an unfolding unit (orange), with ΔG_g of 6.2± 0.2 kcal mol^{-1} and *m*-value of 2.0±0.1 kcal mol^{-1} M^{-1}. The bottom unit (red curves) represents the residues of αE, of which the global unfolding free energy ΔG_g and *m*-value are 5.2± 0.2 kcal mol^{-1} and 1.8±0.1 kcal mol^{-1} M^{-1}, respectively, much lower than the whole structure global unfolding energy ΔG_{H2O}. The free energy αA is higher than that of αF. αA and αB/αD construct one hydrophobic core. αF and αB/αD construct another hydrophobic core. We may speculate that the αA/αB/αD hydrophobic core is much stable than the αB/αD/αF hydrophobic core.

There are some resemblance between partially unfolded states observed at equilibrium and kinetic intermediates for several proteins such as lysozyme [22], cytochrome *c* [23], ribonuclease T_1 [24], and cardiotoxin analogue III [25]. However, it is not universal for all proteins, such as barnase [2] and chymotrypsin inhibitor 2 [26]. Native-state HX is an excellent method for analyzing the equilibrium distribution of unfolded and partly folded states. We have used this method and found 4 cooperative unfolding units of MICAL-1 CH domain. Fersht and co-workers, based on their studies, have showed that there is no obvious relationship between native-state HX at equilibrium and their folding pathways [27]. As the folding pathway of MICAL-1 CH domain is not known, and *m*-values of four units show no obvious difference (representing the sensitivity to denaturant), it is too speculative to discuss the relationship between the 4 cooperative unfolding units and the folding pathway of the CH domain. However, at least, we can say that the present study will shed light on the understanding of the folding pathway.

5. Conclusion

We have performed the hydrogen exchange experiment of MICAL-1 CH domain, and found four distinct unfolding units. We have also found that the hydrophobic core is the slowest exchange core. It may be suggested that hydrophobic interactions are the main force to maintain the three-dimension structure of MICAL-1 CH domain. These findings will be useful for detailed research on folding of MICAL-1 CH domain.

Acknowledgements

We thank all of the members of our laboratory who have contributed to this work. We also thank Dr. F. Delaglio and Prof. A. Bax for providing the software NMRPipe, Prof. T. D. Goddard and Prof. D. G. Kneller for providing Sparky, Dr. Warren L. D. for providing PyMOL. This work was supported by the Chinese National Fundamental Research Project (Grants 2002CB713806 and 2004CB520500), the Chinese National Natural Science Foundation (Grants 30270293, 30121001 and 30570361), and the Pilot Project of

the Knowledge Innovation Program of the Chinese Academy of Science (Grants KSCX1-SW-17 and KJCX2-SW-h14).

References

[1] K.S. Kim, J.A. Fuchs, C.K. Woodward, Hydrogen exchange identifies native-state motional domains important in protein folding, Biochemistry 32 (1993) 9600–9608.
[2] J. Clarke, A.M. Hounslow, M. Bycroft, A.R. Fersht, Local breathing and global unfolding in hydrogen exchange of barnase and its relationship to protein folding pathways, Proc. Natl. Acad. Sci. U. S. A. 90 (1993) 9837–9841.
[3] S.W. Englander, Protein folding intermediates and pathways studied by hydrogen exchange, Annu. Rev. Biophys. Biomol. Struct. 29 (2000) 213–238.
[4] S.W. Englander, L. Mayne, Protein folding studied using hydrogen-exchange labeling and two-dimensional NMR, Annu. Rev. Biophys. Biomol. Struct. 21 (1992) 243–265.
[5] Y. Bai, T.R. Sosnick, L. Mayne, S.W. Englander, Protein folding intermediates: native-state hydrogen exchange, Science 269 (1995) 192–197.
[6] A.K. Chamberlain, T.M. Handel, S. Marqusee, Detection of rare partially folded molecules in equilibrium with the native conformation of RNaseH, Nat. Struct. Biol. 3 (1996) 782–787.
[7] R. Chu, W. Pei, J. Takei, Y. Bai, Relationship between the native-state hydrogen exchange and folding pathways of a four-helix bundle protein, Biochemistry 41 (2002) 7998–8003.
[8] J. Clarke, A.R. Fersht, An evaluation of the use of hydrogen exchange at equilibrium to probe intermediates on the protein folding pathway, Fold. Des. 1 (1996) 243–254.
[9] M. Gimona, K. Djinovic-Carugo, W.J. Kranewitter, S.J. Winder, Functional plasticity of CH domains, FEBS Lett. 513 (2002) 98–106.
[10] E. Korenbaum, F. Rivero, Calponin homology domains at a glance, J. Cell Sci. 115 (2002) 3543–3545.
[11] H. Sun, H. Dai, J. Zhang, X. Jin, S. Xiong, J. Xu, J. Wu, Y. Shi, Solution structure of Calponin Homology domain of Human MICAL_1, J. Biomol. NMR 36 (2006) 295–300.
[12] N. Bhutani, J.B. Udgaonkar, Folding subdomains of thioredoxin characterized by native-state hydrogen exchange, Protein Sci. 12 (2003) 1719–1731.
[13] C.N. Pace, Determination and analysis of urea and guanidine hydrochloride denaturation curves, Methods Enzymol. 131 (1986) 266–280.
[14] J.F. Brandts, H.R. Halvorson, M. Brennan, Consideration of the Possibility that the slow step in protein denaturation reactions is due to cis-trans isomerism of proline residues, Biochemistry 14 (1975) 4953–4963.
[15] M.M. Krishna, L. Hoang, Y. Lin, S.W. Englander, Hydrogen exchange methods to study protein folding, Methods 34 (2004) 51–64.
[16] F. Delaglio, S. Grzesiek, G.W. Vuister, G. Zhu, J. Pfeifer, A. Bax, NMRPipe: a multidimensional spectral processing system based on UNIX pipes, J. Biomol. NMR 6 (1995) 277–293.
[17] Y. Bai, J.S. Milne, L. Mayne, S.W. Englander, Primary structure effects on peptide group hydrogen exchange, Proteins 17 (1993) 75–86.
[18] S.W. Englander, L. Mayne, Y. Bai, T.R. Sosnick, Hydrogen exchange: the modern legacy of Linderstrom-Lang, Protein Sci. 6 (1997) 1101–1109.
[19] S. Hubbard, J.M. Thornton, NACCESS, University College London, London, 1993.
[20] M.M. Santoro, D.W. Bolen, Unfolding free energy changes determined by the linear extrapolation method. 1. Unfolding of phenylmethanesulfonyl alpha-chymotrypsin using different denaturants, Biochemistry 27 (1988) 8063–8068.
[21] Y. Bai, S.W. Englander, Future directions in folding: the multi-state nature of protein structure, Proteins 24 (1996) 145–151.
[22] S.E. Radford, C.M. Dobson, P.A. Evans, The folding of hen lysozyme involves partially structured intermediates and multiple pathways, Nature 358 (1992) 302–307.
[23] H. Roder, G.A. Elove, S.W. Englander, Structural characterization of folding intermediates in cytochrome c by H-exchange labelling and proton NMR, Nature 335 (1988) 700–704.
[24] N.J. Baxter, L.L. Hosszu, J.P. Waltho, M.P. Williamson, Characterisation of low free-energy excited states of folded proteins, J. Mol. Biol. 284 (1998) 1625–1639.
[25] T. Sivaraman, T.K. Kumar, D.K. Chang, W.Y. Lin, C. Yu, Events in the kinetic folding pathway of a small, all beta-sheet protein, J. Biol. Chem. 273 (1998) 10181–10189.
[26] J.L. Neira, L.S. Itzhaki, D.E. Otzen, B. Davis, A.R. Fersht, Hydrogen exchange in chymotrypsin inhibitor 2 probed by mutagenesis, J. Mol. Biol. 270 (1997) 99–110.
[27] J. Clarke, L.S. Itzhaki, A.R. Fersht, Hydrogen exchange at equilibrium: a short cut for analysing protein-folding pathways? Trends Biochem. Sci. 22 (1997) 284–287.